Journal of Food Measurement and Characterization (2023) 17:5594–5605
https://doi.org/10.1007/s11694-023-02045-w

ORIGINAL PAPER

Investigation the interaction between quinoa glycopeptides and polyphenol: spectroscopic analyses and antioxidant activities

Yuyuan Yu[1] · **Yongqing Shi**[1]

Received: 8 March 2023 / Accepted: 3 July 2023 / Published online: 25 July 2023

Abstract

The interaction between quinoa glycopeptides (QGs) and three polyphenols [(−)-epigallocatechin-3-gallate (EGCG), gallic acid (GA) and tannic acid (TA)] was investigated by particle size, potential, fluorescence spectrum, and Fourier infrared spectrum, and the changes of antioxidant activity after compound were investigated by in vitro antioxidant experiments. The results showed that the average particle size of quinoa glycopeptide decreased and its distribution became more uniform after it was combined with three polyphenols. The intrinsic fluorescence was quenched and decreased with the increase of polyphenol content, and the maximum emission wavelength of the intrinsic fluorescence spectrum was redshifted. When combined with EGCG, GA and TA, the surface hydrophobicity of quinoa glycopeptides decreased significantly. The quenching type of EGCG, GA, and TA on quinoa glycopeptides was static quenching. The addition of polyphenols changed the hydrophobic amino acid groups in quinoa glycopeptides, and the hydrophobic interaction was the main force. Additionally, the secondary structure of QG was slightly changed after the binding of polyphenols to QG. Moreover, DPPH and ABTS radical scavenging abilities and ferric reducing antioxidant power analysis showed that EGCG, GA, and TA enhanced significantly the antioxidant capacity of QG. Therefore, this study can guide the preparation of quinoa functional food.

Keywords Quinoa glycopeptides · Polyphenol · Interaction · Antioxidant properties

Introduction

Quinoa is a gluten-free, high-nutrient pseudo-cereal seed crop that can be cultivated in high-salt and dry environments. Because of its good fatty acid profile, high-quality protein, dietary fiber, vitamin, and mineral content, it has received a lot of attention recently [1]. Protein is the main component of quinoa, with an average content of 12–23%. Furthermore, quinoa has a substantially higher composition and amount of critical amino acids than major cereal crops, including wheat, rice, soybean, and corn. Nine essential amino acids for human health are present in quinoa [2]. However, quinoa protein is weak in antioxidation, solubility, and emulsification, which were limited in the functional food process. In order to increase its use in functional foods, quinoa protein is usually processed with physical, chemical, and biological processes to form quinoa protein hydrolysates. Quinoa protein hydrolysate can increase antioxidation, antimicrobial activity, and antihypertensive effects [3]. Microbial fermentation can improve the biological activity of quinoa protein. During fermentation, microbes can release enzymes that can break proteins down into smaller molecules with physiological functions, such as peptides, amino acids, and other nitrogen-containing substances [4]. However, hydrolysis is a complex and challenging process to govern. Bioactive peptides must be obtained by limited or regulated hydrolysis. More focus has been placed on the creation of suitable techniques to increase the biological activity of hydrolysates.

There are one or two aromatic rings with one or more hydroxyl substituents in phenolic compounds, which are important natural substances that are abundantly present in plants and created in the metabolic process of plants under the impact of their environment [5]. They exhibit a variety of biological activities, including antibacterial and antioxidant properties. Most phenolic compounds are natural antioxidants that can postpone oxidizing damage.

✉ Yongqing Shi
shiyq@zjsu.edu.cn

Yuyuan Yu
yuyuyuan98@163.com

[1] College of Food Science and Biotechnology Engineering, Zhejiang Gongshang University, No. 18, Xuezheng Street, Hangzhou 310018, China

Numerous biochemical and molecular biology investigations have demonstrated that phenolic compounds can alter the physical chemistry and functional properties of proteins, including emulsification, digestibility, thermostability, and antioxidant activity [6].

Covalent and non-covalent interactions between polyphenols and proteins can alter the secondary structure of proteins and improve their functionality. For instance, the non-covalent binding of chlorogenic acid to whey protein or casein increased free radical scavenging and digestibility [7]. The emulsifying and antioxidant capabilities of soy protein bound to (−)-Epigallocatechin-3-gallate (EGCG) by hydrophobic interaction and hydrogen bonding can be greatly enhanced [8]. The combination of lactoferrin and tannic acid (TA) increased significantly the antioxidant activity ($p < 0.05$) and showed better inhibitory effects on *Bacillus subtilis* and *Saccharomyces cerevisiae* [9]. Duck albumen hydrolysates (DAH) were conjugated with EGCG at different concentrations, which increased the surface hydrophobicity of DAH and improved its antioxidant and emulsifying capabilities [10]. According to these studies, polyphenols interact with proteins or peptides to form complexes that enhance antioxidant activity.

Although the use of polyphenols to enhance the antioxidant activity of quinoa proteins has been studied, the antioxidant effect of polyphenols on quinoa glycopeptides (QG) is still not fully understood. Therefore, in this study, QG derived from quinoa fermentation liquid were used to prepare non-covalent complexes with polyphenols (EGCG, GA, and TA). The structures of QG, polyphenols, and QG–polyphenols complexes were investigated with fluorescence spectroscopy and Fourier transform infrared spectroscopy (FTIR). The antioxidant activity of quinoa glycopeptides was investigated by ABTS, DPPH radical scavenging activities, and ferric reducing antioxidant power (FRAP). It is hoped that the pharmaceutical and functional food industries would find this study interesting.

Materials and methods

Materials

Mucor wutungkiao (CICC 3109) and *Rhizopus oryzae* (CICC 41214) were previously isolated and are stored at China Industrial Microbial Species Preservation Center (CICC). Quinoa was obtained from Ge'ermu Namulan Trading Co., Ltd. (Gansu, Qinghai, China). EGCG and GA at over 98% purity, as determined by HPLC, was purchased from Mclean Biotechnology Co., Ltd. (Shanghai, China). TA was analytically pure, purchased from Damao Chemical Reagent Factory (Tianjin, China). α-Amylase (10,000–20,000 U/g) was purchased from Nanning Pombo bioengineering limited (Nanning, China). 8-anilino-1-naphthalenesulfonic acid (ANS), 2,2-diphenyl-1-picrylhydrazyl (DPPH), 2,2′-Azinobis (3-ethylbenzothiazoline-6-sulfonic acid (ABTS) and ascorbic acid were acquired from Aladdin Chemical Co. LTD (Shanghai, China). Other reagents and chemicals used were of analytical grade and obtained from Sinopharm Chemical Reagent Co. LTD (Shanghai, China).

Preparation of quinoa glycopeptides

Quinoa glycopeptides were prepared based on our previous studies. Quinoa had been cleaned and sorted in distilled water until no froth was created, then dried in a hot air oven set at 40 ℃ for 6 h. The washed quinoa seeds were soaked in distilled water at room temperature (25 ± 2 ℃) for 12 h (1:18 w/v) to fill it with moisture, and then the quinoa seeds were blended using an attrition mill (JYL-CO2OE model, Joyoung, China). The quinoa homogenate samples were hydrolyzed for 40 min at 80 ℃ with 1% (w:w) α-amylase to remove starch. Then the α-amylase hydrolysates were immediately heated for 10 min at 100 ℃ to stop the enzyme reaction. After cooling to room temperature (25 ℃), the starch-free quinoa homogenate samples were distributed in sterile screw-top glass bottles (550 mL) in an ultraclean desk. Then *Mucor* and *Rhizopus oryzae* were inoculated into the bottles with an inoculum size of 1.4×10^5 CFU/mL. They were fermented for 8.7 days at 28 ℃ for the production of quinoa hydrolysate. The quinoa hydrolysate was filtered with filter paper to eliminate large particles, then centrifuge the filtrate at 10,000 r/min for 10 min to obtain fermentation supernatant. Ethanol was then added to the fermentation supernatant until it was 80% by total volume, and the mixture was then left at 4 ℃ for 12 h to obtain the crude quinoa glycopeptides precipitates. The resulting precipitates were then freeze-dried and stored at − 40 ℃ for subsequent analysis.

Crude quinoa glycopeptides (100 mg) were dissolved in 1.0 mL of ultrapure water and separated with a Sephadex G-15 gel filtration chromatography column (16 × 600 mm), with ultrapure water serving as the eluent and an elution flow rate of 12 drops/min. The peptides elution curve was obtained by measuring the absorbance at 280 nm with a UV detector (HD-5, Shanghai Huxi, China). The content of polysaccharides in each tube was monitored by the phenol–sulfuric acid method, and the elution curve of polysaccharides was drawn. The fractions corresponding to the overlapping peaks of the two elution curves were collected. Then each fraction (2 mg/mL) was tested for DPPH radical scavenging activity, ABTS radical scavenging activity and ferric reducing power, and the most active fraction was chosen for glycopeptide–polyphenol complex preparation. Fractions with high antioxidant activity were collected repeatedly, then freeze-dried and stored at − 40 ℃.

Preparation of QG–polyphenol complex

All samples were prepared according to the method of Dai et al. [11] with some slight modifications. To make the quinoa glycopeptide solution (100 mg/mL), quinoa glycopeptide powder was dissolved in distilled water. Then the polyphenols of different weight (1 mg, 1.67 mg, 3.33 mg, 5 mg, 10 mg and 20 mg) were weighed and dissolved in 4.9 mL of distilled water. The quinoa glycopeptides solution (0.1 mL) was injected slowly into different polyphenol solutions under continuous magnetic stirring at 150 r/min for 120 min at room temperature (25 ± 2 ℃). The final QG–polyphenol mass ratios were 10:1, 6:1, 3:1, 2:1, 1:1, and 1:2, respectively.

Particle size and ζ-potential

The particle size, polydispersity index (PDI), and ζ-potential of the complexes were determined according to the method of Dai et al. [9]. An AZ-sizer nano ZS (Malvern Instruments, Worcestershire, UK) equipped with dynamic light scattering (DLS) was used to get the data from freshly prepared samples. All samples were balanced for 120 s at 25 °C and measured three times.

UV–Vis absorption spectroscopy

The samples (QG and QG–polyphenol complex) were diluted with distilled water. The final concentration of QG in each sample was 0.2 mg/mL. The QG-polyphenol system was monitored using the UV–Vis spectrophotometer (UV-2600, Shimadzu, Japan) scanning over the wavelength range of 200–400 nm according to the modified method of Parolia et al. [12].

Fluorescence spectroscopy analysis

The fluorescence emission spectra of the samples were measured by a fluorescence spectrometer (F-7000, HITACHI, Tokyo, Japan) according to the method of Liu et al. [13]. Different samples (QG, QG–polyphenol complex) were dissolved in distilled water. The final concentration of QG in each sample was 0.02 mg/mL. The excitation wavelength was 260 nm, and the scanning range was 300–450 nm. The excitation and emission slit widths were 5 nm.

Surface hydrophobicity

The impact of polyphenol on the surface hydrophobicity of QG-polyphenol was determined by a fluorescence spectrofluorometer (F-7000, HITACHI, Tokyo, Japan) according to the method of Dai et al. [9] with some modifications. All samples were dissolved in distilled water. The final concentration of QG in each sample was 0.02 mg/mL. Aliquots of QG or QG-polyphenol (4 mL) were added to 20 µL of ANS solution (8 mmol/L), which was then reacted in a dark place for 3 min. The excitation wavelength was 390 nm, the emission wavelength range was 400 to 700 nm, and the widths of the excitation and emission slits were 5.0 nm.

Fourier transform infrared spectroscopy

The secondary structure of QG or QG–polyphenol complex was measured using an infrared spectrometer (NICOLETIS5, Thermo-Scientific, Germany) according to the method of Han et al. [14]. A 2 mg sample and 200 mg of potassium bromide were mixed and beaten into a transparent sheet with a mold. The wavelength range was 400–4000 cm^{-1} with 32 scans at a resolution of 4 cm^{-1}. The OMNIC 8.2 software was used for the data analysis.

Antioxidative properties of the QG–polyphenol complex

DPPH radical scavenging activity

The DPPH radical scavenging activity of the sample was determined according to the method of Wang et al. [15] with some slight modifications. DPPH–ethanol solution (40 mg/mL) was prepared and stored at 4 ℃ in the dark. Different samples (QG–EGCG complex, QG–GA complex, and QG–TA complex) were dissolved in distilled water, and the final concentration of QG in each sample was 0.033 mg/mL, 0.02 mg/mL, and 0.033 mg/mL, respectively. A 20 µL portion of sample was mixed with DPPH–ethanol solution (180 µL). Then, the mixtures were stored in the dark at 37 ℃ for 60 min. DPPH–ethanol solution which received no sample were used as controls. The absorbance was determined at 517 nm by enzyme-labelled instrument (spectraMax Plus 38, Molecular Devices, USA). The DPPH free radical scavenging activity was calculated from the following formula:

$$\text{DPPH radical scavenging activity}(\%) = \left(1 - \frac{A_1 - A_2}{A_0}\right) \times 100\% \quad (1)$$

where A_1 is the absorbency of sample + DPPH–ethanol solution, A_2 is the absorbency of sample + ethanol solution and A_0 is the absorbency of distilled water + DPPH–ethanol solution.

ABTS radical scavenging activity

The ABTS radical scavenging activity of the sample was determined according to the previously reported method of Wang et al.[15] with some slight modifications. The ABTS working solution, which was consisted of equal volumes of

ABTS (7 mmol/L) solution prepared with phosphate-buffered saline (PBS, 5 mmol/L, pH7.4) and oxidant solution (2.45 mmol/L) prepared with PBS, was stored in the dark at 25 ℃ for 16 h, and then it was dissolved in PBS buffer to an absorbance of 0.7 ± 0.02 at 734 nm. Different samples (QG–EGCG complex, QG–GA complex, and QG–TA complex) were dissolved in distilled water, and then the final concentrations of QG in each sample was 0.033 mg/mL, 0.02 mg/mL, and 0.033 mg/mL, respectively. A 25 μL portion of each sample was reacted with ABTS-ethanol solution (175 μL). All the mixtures were stored in the dark at 37 ℃ for 10 min. The ABTS working solution without sample was used as control. The absorbance was determined at 734 nm by enzyme-labelled instrument. The ABTS free radical scavenging activity was calculated according to the following formula:

$$\text{ABTS radical scavenging activity}(\%) = \left(1 - \frac{A_1 - A_2}{A_0}\right) \times 100\% \quad (2)$$

where A_1 is the absorbency of sample + ABTS working solution, A_2 is the absorbency of sample + distilled water and A_0 is the absorbency of distilled water + ABTS working solution.

Ferric reducing antioxidant power (FRAP)

The FRAP of the samples were determined as described method of Wang et al.[15] with some modification. Different sample (QG–EGCG complex, QG–GA complex, and QG–TA complex) were dissolved in distilled water. The final concentrations of QG in each sample were 0.2 mg/mL, 0.1 mg/mL, and 0.2 mg/mL, respectively. The 1 mL sample was mixed with 2.5 mL of PBS (pH 6.8, 0.01 mol/L) and 3 mL of $K_3[Fe(CN)_6]$ (10 mg/mL). The mixtures were incubated at 50 ℃ for 20 min. Then 2.5 mL of trichloroacetic acid (100 mg/mL) was added. Then the mixture was centrifuged at 5000 r/min for 10 min. Subsequently, the supernatant (2.5 mL) was mixed with 2.5 mL of distilled water and 0.5 mL of $FeCl_3$ (0.1%). The absorbance of each sample at 700 nm was measured to describe the ferric reducing power. A Vc calibration curve was formulated in the concentration range 0.01–0.80 mg/mL following the same method as described above. The final value is expressed as the Vc concentration. VC standard curve equation: $y = 0.1594x + 0.0812$, $R^2 = 0.999$.

Statistical analysis

All experiments were performed in triplicate. Mean values and standard errors of triplicate data were performed. Statistical analyses were conducted by ANOVA with SPSS 26.0 (SPSS Inc., Chicago, IL, USA). When the results were significant, the Duncan's multiple range tests were also used. A probability level of $p < 0.05$ was used in testing statistical significance.

Results and discussion

Separation and purification of QG

As shown in Fig. 1A, the crude glycopeptide was eluted by sephadexG-15. Four elution peaks appeared at 280 nm, and were denoted by A, B, C, and D. The four components were gathered repeatedly and freeze-dried. The antioxidant activity of all samples (2 mg/mL) was determined. As shown in Fig. 1B, the antioxidant activity of component A, B, and D was significantly lower than that of component C ($p < 0.05$), and the content of component C was higher than all the other components. As a result, component C was repeatedly gathered for further examination.

Particle size and ζ-potential

Figure 1C shown the particle size and PDI of QG, EGCG, and QG–EGCG complex. The particle sizes of the QG and EGCG nanoparticles were 696.4 ± 144.18 nm and 455.43 ± 90.23 nm, respectively. It was discovered that the particle size of QG–EGCG complex nanoparticles was smaller than the particle size of QG nanoparticles or EGCG nanoparticles. This was probably due to the interaction between QG and EGCG, in which the spatial structure of QG was changed and a stable colloidal particle distance was formed, thus affecting QG self-assembly [16]. As the EGCG addition ratio rose, the particle size of QG–EGCG complex nanoparticles initially decreased, then increased. When the level of EGCG increased (the ratio of QG to EGCG changed from 10:1 to 6:1), the particle size decreased from 214.30 ± 36.16 nm to 188.35 ± 14.19 nm. However, when the EGCG level was raised (the ratio of QG to EGCG changed from 6:1 to 1:2), the particle size increased from 188.35 ± 14.19 nm to 444.5 ± 40.26 nm. The variation in nanoparticle size demonstrated that the surface characteristics of QG were connected to the interaction between polyphenol and protein. Similar changes in the PDI value and particle size indicated that the composite nanoparticles were stable. The potential value of QGs and EGCG composite has not changed significantly.

The particle size and PDI of the QG, GA, and QG–GA complex were presented in Fig. 1D. The particle size and PDI of nanoparticles were considerable when only GA was present. It was indicated that this was a system with an unstable and uneven size distribution of the colloidal particles. The particle sizes of the QG–GA complex nanoparticles were smaller than those of the monomeric

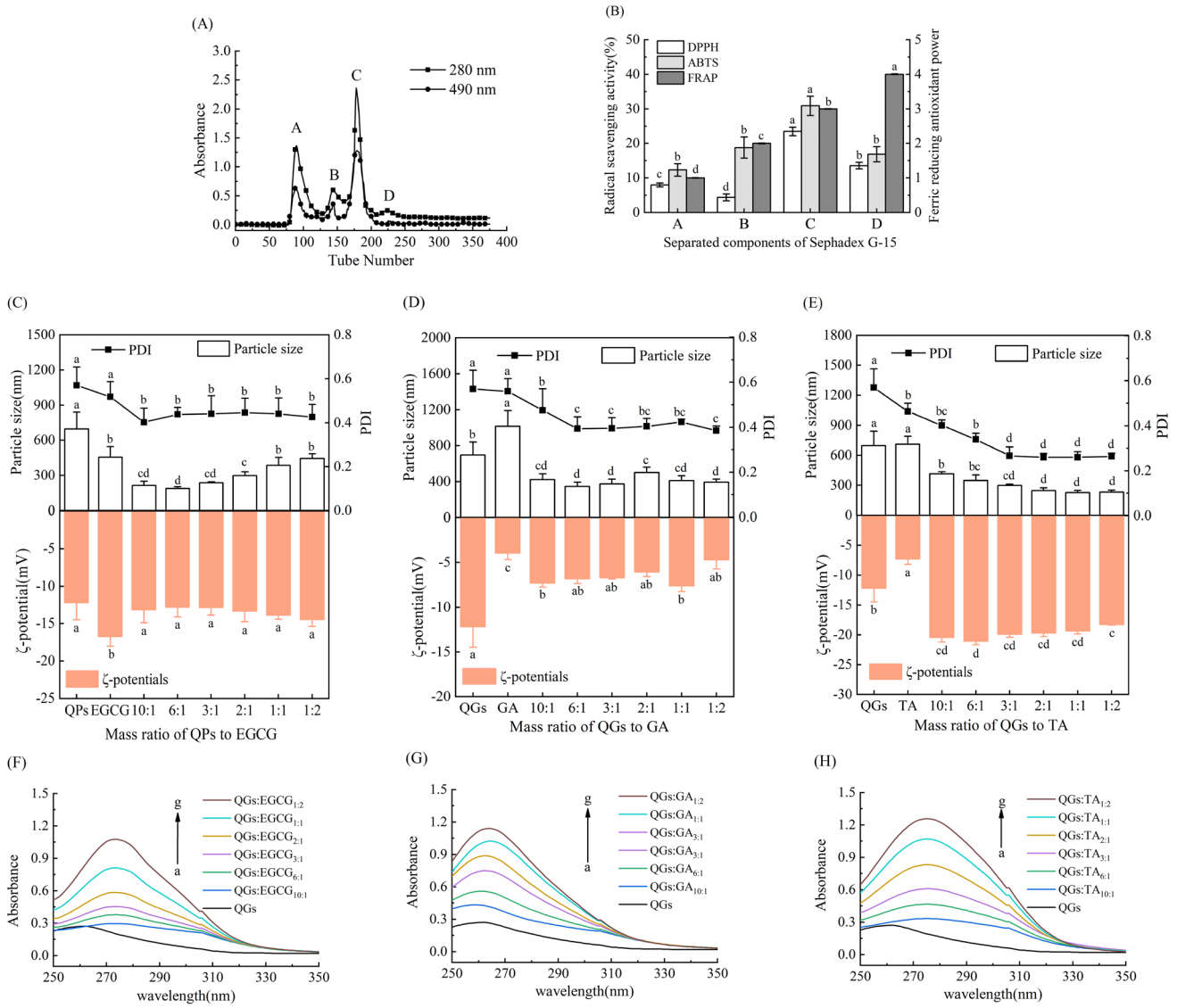

Fig. 1 **A** is the separation and purification by Sephadex G-15. **B** is the antioxidant activity analysis of separated components of Sephadex G-15, a, b, c and d indicating significant differences between different components. **A** is the separation and purification by Sephadex G-15. **B** is the antioxidant activity analysis of separated components of Sephadex G-15, a, b, c and d indicating significant differences between different components. **C**, **D** and **E** are the particle size, polydisperse index (PDI) and ζ-potential of QG–polyphenol complexes (EGCG, GA, and TA). QG means Quinoa glycopeptides. 10:1, 6:1, 3:1, 2:1, 1:1 and 1:2 represent the mass ratio of QG and EGCG, GA or TA, respectively. (**F**), (**G**) and (**H**) represent UV–Vis absorption spectra of QG and QG-polyphenol (EGCG, GA and TA) complexes in different mass ratios. a→g: represents the mass ratio of QG to EGCG, GA or TA respectively (10:1, 6:1, 3:1, 2:1, 1:1, 1:2), respectively

QG and GA nanoparticles. Yi et al. [17] found that the particle size of soybean protein isolate nanoparticles or GA nanoparticles shrank steadily as the GA concentration increased. Moreover, the potential value decreased after the two substances were mixed, which indicated that the two substances constituted a stable complex. Emulsions with low zeta potential had a propensity to coagulate or flocculate. Whereas emulsions with high zeta potential (positive or negative) were electrically stable [18]. The ζ-potential value increases gradually after being compounded with QG, demonstrating that QG–GA is stable.

The particle size and PDI of QG, TA, and QG–TA complex were displayed in Fig. 1E. The effect of TA on QG was similar to that of EGCG on QG, and the size of complex nanoparticles was smaller than that of nanoparticles containing only QG or GA. The particle size and PDI value of QG–TA nanoparticles steadily decreased with a rise in the TA addition ratio, indicating that the complex gradually

became more stable. This might be because a stable distance had been built between QG and TA [16]. When the TA concentration was less than 8 mg/mL, Zhan et al. [19] described that the particle size of the complex shrank with increasing concentration. The ζ-potential value of the complex was significantly lower than that of the single particle ($p < 0.05$), indicating that the complex particle was more stable.

In summary, when proteins bound to polyphenols at low polyphenol concentrations, it was easier to form smaller particles. Moreover, some polyphenols could act as cross-linking agents between protein molecules in high quantities, causing proteins to aggregate and precipitate.

UV–Vis spectra

UV–Vis spectroscopy was an effective method to monitor changes in protein structure. Tyrosine, phenylalanine, tryptophan, and sulfur-containing amino acids had absorption peaks in the range of 230–310 nm. Tryptophan and tyrosine residues had a conjugated double bond that exhibited an absorption peak at 280 nm, whereas phenylalanine had a characteristic absorption peak near the wavelength of 257 nm [20]. As shown in Fig. 1F and G the QG solution had an obvious UV absorption peak at 260 nm wavelength, which was related to the secondary structure and microenvironment of tryptophan (Trp), tyrosine (Tyr), and L-phenylalanine (Phe) residues. With the addition of EGCG, GA, or TA to QG solution, the absorption intensity of QG increased, and the maximum absorption wavelength red-shift indicated that the hydrophobicity decreased after the addition of EGCG, GA, or TA. Similar results were reported by Yan et al. [21] that the UV absorption value of camphor seed protein increased with the increase of camphor polyphenols, and the red shift occurred after the addition of polyphenols.

Fluorescence spectroscopy

The interaction between protein and ligand, which was reflected by the change in fluorescence intensity of protein emission after adding ligand, can be studied using the fluorescence spectrum. Proteins give off intrinsic fluorescence because they contain tyrosine, tryptophan, and L-phenylalanine residues. The fluorescence was quenched when the ligand attached to these chromophores. Moreover, the ligand bound to different protein locations may alter the protein to expose or hide the chromophores and alter the emission of intrinsic fluorescence [1]. The fluorescence spectra of QG, QG–EGCG complex, QG–GA complex, and QG–TA complex were shown in Fig. 2. QG had a maximum fluorescence intensity at an emission wavelength of 330 nm, which was similar to the emission wavelength at which quinoa protein had a maximum fluorescence intensity [22]. The interaction between QG and polyphenols was indicated by the fact that the fluorescence intensity of QG diminished when the ratios of EGCG, GA, or TA increased. The maximal emission peak of QG appeared to undergo a clear red-shift when QG was complexed with EGCG, GA, or TA, moving from 330 to 332 nm, 330 nm to 346 nm, and 330 nm to 338 nm, respectively. When the aromatic ring on the phenol interacted with the hydrophobic area of the QG, the microenvironment became less hydrophobic,

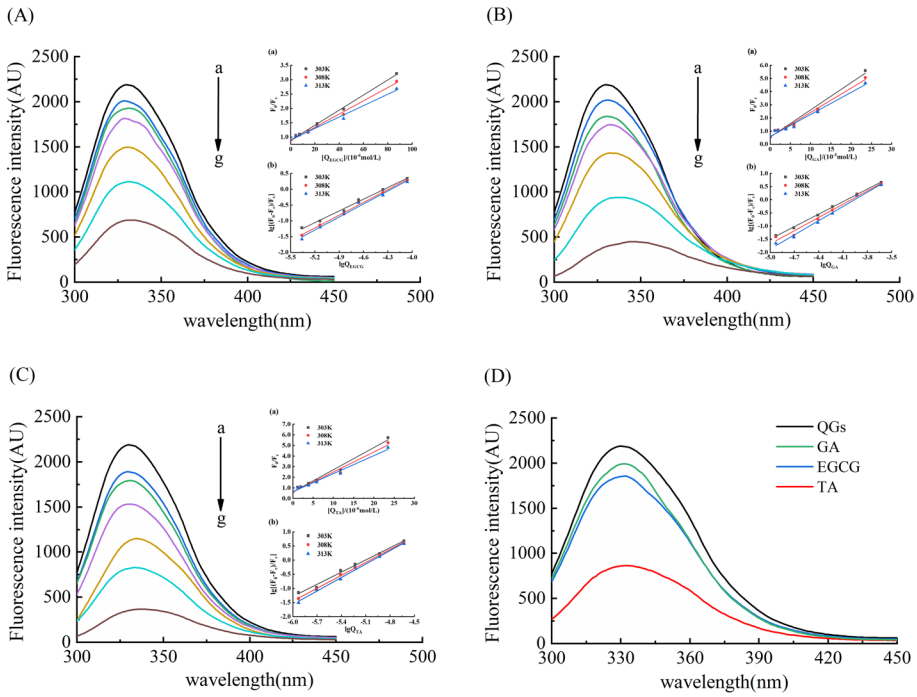

Fig. 2 Fluorescence spectra of QG (0.02 mg/mL) treated with different concentrations of EGCG (**A**), GA (**B**) and TA (**C**) (a → g: 0.002, 0.00334, 0.00667, 0.01, 0.02, and 0.04 mg/mL) at T = 303 K, pH 7.0. (**D**) Fluorescence spectra of QG (0.02 mg/mL) treated with EGCG, GA, and TA (1×10^{-5} mol/L). Insets: (a) Stern–Volmer plots of QG with polyphenol added at 303, 308, and 313 K. (b) The plots for the static quenching of QG by polyphenol at 303, 308, and 313 K

and the intrinsic chromophore was exposed to a more hydrophilic environment [23]. These studies pointed out that the addition of polyphenols led to the exposure of tryptophan residues and the unfolding of proteins, resulting in a decrease in fluorescence intensity and a redshift of the maximum emission peak of proteins[7].

Furthermore, as shown in Fig. 2D, when the concentration of polyphenols was 1×10^{-5} mol/L, the addition of TA caused the largest reduction in the fluorescence intensity of QG, followed by EGCG, and then GA. This might be related to the aromatic ring and O–H in the polyphenol structure. TA and EGCG were abundant in active sites, shielding effects, and polar enhancers, as well as having a sizable quenching capacity [24].

In dynamic quenching, the chromophore group was stopped from emitting fluorescence by the quenching agent, and the quenching constant rose as the temperature rose. In static quenching, the chromophore group and the quenching agent form a complex, and the static binding constant fell as the temperature rose [8].

The fluorescence measurements of QG and its complexes were adjusted using the following equation to get rid of the inner-filter effects [25]:

$$F = F_1 e^{\frac{A_{ex}+A_{em}}{2}} \tag{3}$$

where F is the corrected fluorescence intensity, F_1 is the observed fluorescence intensity, and A_{ex} and A_{em} are the ultraviolet visible absorption values of EGCG, GA, and TA at the excitation wavelength of 260 nm and the emission wavelength of 330 nm, respectively.

The Stern–Volmer equation can be used to assess the data on fluorescence quenching at various temperatures [11]. Then the types and mechanisms of QG and fluorescence quenching by EGCG, GA, and TA can be further discussed.

$$\frac{F_0}{F} = 1 + K_q \times \tau_0 \times [Q] = 1 + K_{SV} \times [Q] \tag{4}$$

where F_0 means the fluorescence intensity without EGCG, GA, and TA, F means the corrected fluorescence intensity, K_q means the fluorescence quenching rate constant, τ_0 is 10^{-8} s [26], which means the fluorescence lifetime of the fluorophore in the absence of the quenching agent, Q is the concentration of polyphenols, and K_{SV} is the quenching constant of the Stern–Volmer equation.

The relevant quenching parameters Table 1 and the Stern–Volmer curve at different temperatures were obtained (Fig. 2) according to the Stern–Volmer equation. Based on these results, the practical quenching mechanism was elucidated. The K_q values peaked at 10^{12} L/(mol/s), more significantly than 2×10^{10} L/(mol/s) reported by Zhang et al. [26]. Therefore, the quenching mechanism of the three polyphenols (EGCG, GA, and TA) for QG was thus regarded as a static one. Furthermore, TA had a greater fluorescent quenching capacity than EGCG and GA.

Binding constants and site numbers were important quantitative data for studying the interaction between small molecules and proteins. Static quenching equations could be used to obtain information on the noncovalent interactions between QG and polyphenols [11].

$$lg\frac{F_0 - F}{F} = lgK_a + nlg[Q] \tag{5}$$

where Ka is the binding constant and n is the number of binding sites.

As shown in Table 1, the n values were all approximately unity, which suggested that EGCG, GA, and TA interact with QG to form complexes with a 1:1 M ratio. The binding constants of QG with EGCG, GA, and TA range from 10^5 to 10^7 L/mol, indicating that the QG–EGCG complex, QG–GA complex, and QG–TA complex were relatively stable. Moreover, the Ka values of the three complexes increased with temperature, suggesting that complexation became more favorable at

Table 1 Quenching constants (K_{sv}, K_q and K_a), number of binding sites (n) and thermodynamic parameters (ΔH, ΔS and ΔG) at 303, 308, and 313 K of QG-polyphenol non-covalent complexes

Complexes	T (K)	K_{SV} (L/mol/S)	R^2	K_q (L/mol/S)	K_a (L/mol)	n	ΔH (kJ/mol)	ΔS (J/(mol K))	ΔG (kJ/mol)
QG–EGCG	303	$(2.63\pm0.07)\times10^4$	0.99	$(2.63\pm0.07)\times10^{12}$	2.20×10^5	1.23	86.71	389.90	−31.10
	308	$(2.31\pm0.08)\times10^4$	0.99	$(2.31\pm0.08)\times10^{12}$	5.98×10^5	1.35			−34.06
	313	$(1.98\pm0.09)\times10^4$	0.98	$(1.98\pm0.09)\times10^{12}$	6.88×10^5	1.37			−34.98
QG–GA	303	$(2.07\pm0.11)\times10^4$	0.98	$(2.07\pm0.11)\times10^{12}$	2.62×10^6	1.58	126.09	538.58	−37.23
	308	$(1.85\pm0.10)\times10^4$	0.98	$(1.85\pm0.10)\times10^{12}$	5.08×10^6	1.68			−39.54
	313	$(1.68\pm0.09)\times10^4$	0.98	$(1.68\pm0.09)\times10^{12}$	1.30×10^7	1.80			−42.62
QG–TA	303	$(2.09\pm0.11)\times10^5$	0.98	$(2.09\pm0.11)\times10^{13}$	2.19×10^7	1.44	112.24	511.19	−42.58
	308	$(1.89\pm0.12)\times10^5$	0.97	$(1.89\pm0.12)\times10^{13}$	4.96×10^7	1.52			−45.38
	313	$(1.70\pm0.09)\times10^5$	0.98	$(1.70\pm0.09)\times10^{13}$	9.07×10^7	1.59			−47.68

higher temperatures. This might have occurred because hydrophobic interactions get stronger as the temperature is raised [27].

The interactions between the protein and ligand mainly included hydrogen bonds, hydrophobic interactions, Johannes Diderik van der Waals forces, and electrostatic interactions, which could be judged by thermodynamic parameters. The thermodynamic parameters were calculated by the Van't Hoff formula, and the interaction between protein and ligand can be further determined [11].

$$\ln K_a = -\frac{\Delta H}{RT} + \frac{\Delta S}{R} \tag{6}$$

$$G = -RT \ln K_a \tag{7}$$

where Ka is the binding constant, R is the gas constant, 8.314 J/(mol K). When ΔG is less than 0, the combination of protein and ligand can proceed spontaneously. When $\Delta H < 0$ and $\Delta S < 0$, the forces between protein and ligand are mainly hydrogen bonds and van der Waals forces. When $\Delta H > 0$ and $\Delta S > 0$, the forces between protein and ligand are mainly hydrophobic interaction. When $\Delta H < 0$ and $\Delta S > 0$, the forces between protein and ligand are mainly electrostatic interaction [25].

The values of ΔG, ΔS, and ΔH were shown in Table 1. The negative ΔG values indicated that binding was spontaneous, and the negative ΔS and ΔH values indicated that binding between QG and selected polyphenols was driven primarily by hydrophobic interactions. Previous researchers had reported that hydrophobic interactions were the main driving force involved in the formation of the zein–EGCG complex [13].

Synchronous fluorescence

Surface hydrophobicity could reflect the number of hydrophobic groups exposed to the surface of a protein, which was related to the number of non-polar amino acid groups contacted by the surrounding water and plays an important role in surface-related functions of proteins. In this study, ANS was employed as a fluorescence probe to evaluate the surface hydrophobicity of the complexes. As shown in Fig. 3, the surface hydrophobicity of QG decreased significantly when it was combined with different polyphenols (EGCG, GA, or TA). The surface hydrophobicity of the QG–EGCG complex did not increase with the amount of EGCG (Fig. 3A). This was consistent with the effect of procyanidin on the surface hydrophobicity of rice glutenin reported by Dai et al. [28]. The surface hydrophobicity of QG decreased while the proportion of GA or TA was added, as shown in Fig. 3B and C. These results indicated that the decrease in surface hydrophobicity of QG was closely related to structural change. One possible reason was that more hydrophilic groups were exposed due to the binding of hydrophobic parts of polyphenols and QG. Another reason was that the number of hydrophilic groups in polyphenols (such as OH and COOH) attached to the surface of QG increases [27].

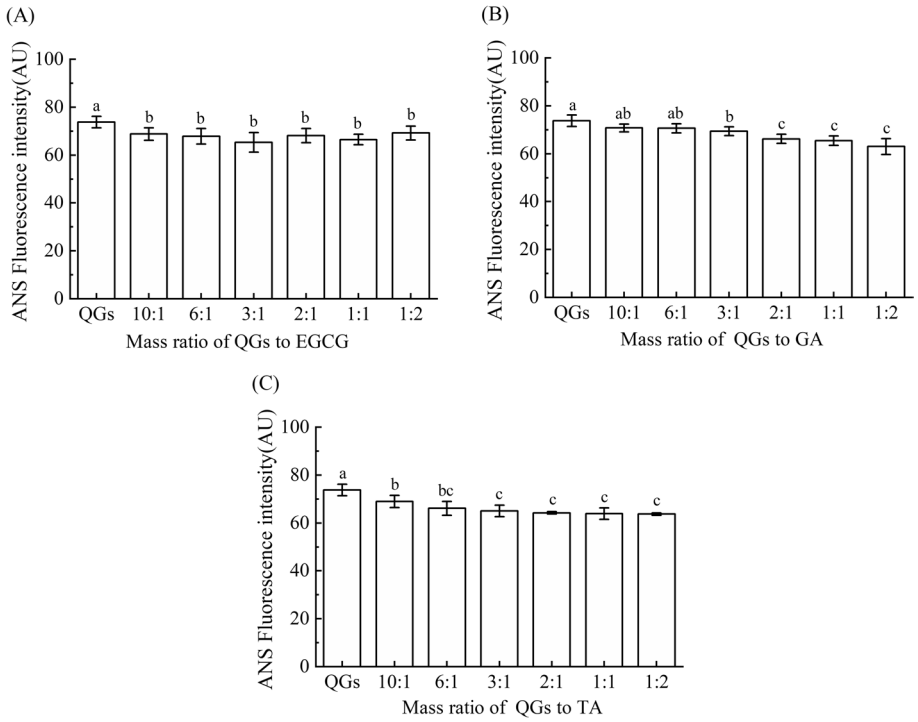

Fig. 3 **A**, **B** and **C** are the surface hydrophobicity of QG and QG–polyphenol (EGCG, GA and TA) non-covalent complexes in different mass ratios, respectively. 10:1, 6:1, 3:1, 2:1, 1:1 and 1:2 represent the mass ratio of QG and EGCG, GA or TA, respectively

FTIR analysis

FTIR spectroscopy was a common method to study the changes in protein secondary structure. Typical protein absorption peaks for QG were at 3428 nm (O–H stretching), 2934 nm (C–H stretching), 1650 nm (C=O stretching), and 1548 nm (C–N stretching, C–C, and N–H bending) [2]. While in the spectra of QG–polyphenol complexes, the shape and peak position of these absorption bands had changed. Figure 4D shown the FTIR analysis of QG, EGCG, and the QG–EGCG complex. The peak positions shifted in different degrees, from 3428 to 3359 cm^{-1}, indicating that QG and EGCG interact in different degrees. Moreover, the extent of the interaction between them was related to the amount of EGCG added. The more EGCG that was added, the greater the peak shift. The stretching vibration peak of C–H showed a blue-shift, and the peak intensity decreased gradually, which indicated that the hydrophobic interaction between QG and EGCG occurred during the formation of the complex and that the surface hydrophobicity of QG decreased. However, at high EGCG concentrations, the stretching vibration peak of C-H shifts to the longer wavelength direction, which might be due to the aggregation of QG induced by high EGCG concentrations and the inhibition of the hydrophobic interaction between EGCG and the hydrophobic groups in QG [9]. The trends of the maximum peaks of the QG–GA complex and the QG–TA complex were similar to those of the QG–EGCG complex (Fig. 4E, F).

When changes in protein secondary structure were evaluated, the amide I band was more sensitive than the amide II band. The amide I band (1600–1700 cm^{-1}) was used to investigate QG secondary structure (α-helix, β-sheet). 1610–1640 cm^{-1} was β-sheet, 1640–1650 cm^{-1} was random

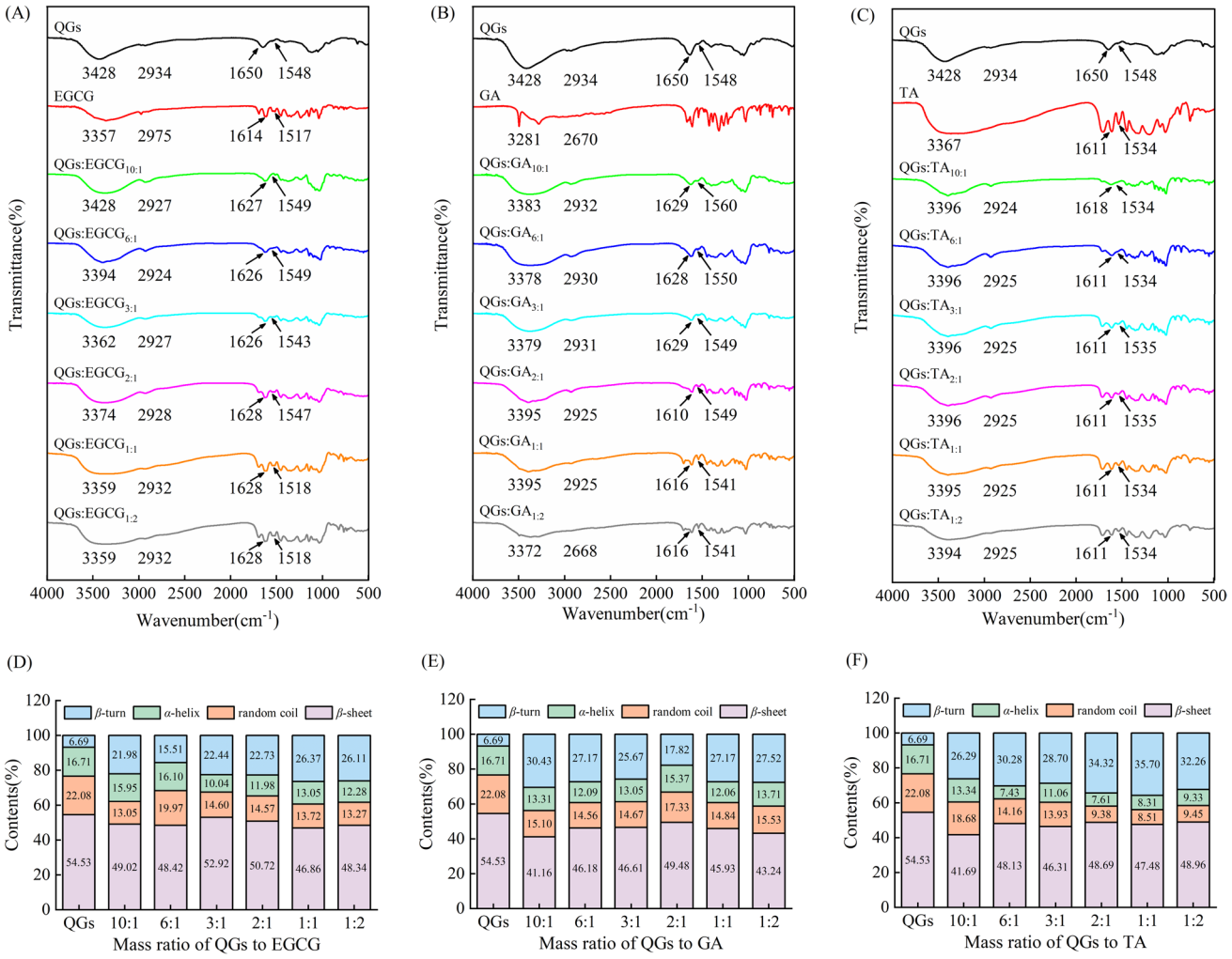

Fig. 4 **A**, **B** and **C** are the FTIR spectra of QG–EGCG, QG–GA and QG–TA non-covalent complexes under different mass ratios, respectively. **D**, **E** and **F** are the Secondary structures of QG–EGCG, QG–GA and QG–TA non-covalent complexes, respectively. 10:1, 6:1, 3:1, 2:1, 1:1 and 1:2 represent the mass ratio of QG and EGCG, GA or TA, respectively

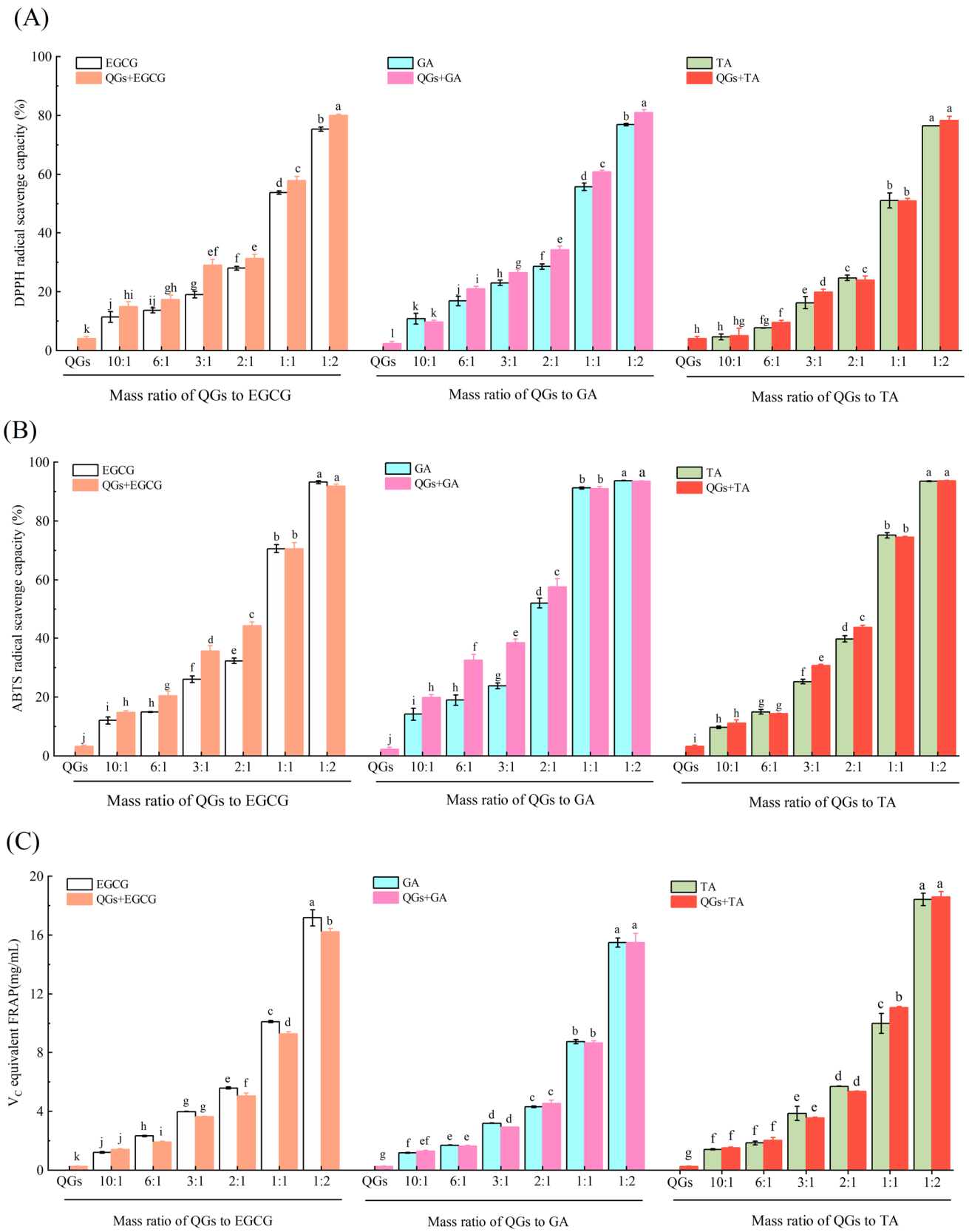
(A)
DPPH radical scavenge capacity (%)
EGCG
QGs+EGCG
GA
QGs+GA
TA
QGs+TA
QGs
10:1
6:1
3:1
2:1
1:1
1:2
Mass ratio of QGs to EGCG
Mass ratio of QGs to GA
Mass ratio of QGs to TA
(B)
ABTS radical scavenge capacity (%)
(C)
V_C equivalent FRAP(mg/mL)

◂**Fig. 5** **A** DPPH radical scavenging activity of QG and QG-polyphenol (EGCG, GA and TA) non-covalent complexes with different mass ratios. **B** ABTS radical scavenging activity of QG and QG-polyphenol (EGCG, GA and TA) non-covalent complexes with different mass ratios. **C** Ferric reducing antioxidant power of QG and QG-polyphenol (EGCG, GA and TA) non-covalent complexes with different mass ratios. Antioxidant activity of QG and QG-polyphenol (EGCG, GA and TA) complexes with different mass ratios. 10:1, 6:1, 3:1, 2:1, 1:1 and 1:2 represent the mass ratio of QG and EGCG, GA or TA, respectively

coil, 1650–1660 cm^{-1} and 1660–1695 cm^{-1} was α-helix and β-turn respectively [14]. Based on FTIR analysis, the β-turn contents of the QG–EGCG complex, QG–GA complex, and QG–TA complex compared to the QG increased from 6.69 to 26.11%, 27.52%, and 32.26%, respectively. Conversely, the β-sheet contents of the QG–EGCG complex, QG–GA complex, and QG–TA complex compared to the QG decreased from 54.53 to 48.34%, 43.24%, and 48.96%, respectively. This result indicated that the non-covalent binding of EGCG, GA, and TA to proteins led to a change in the secondary structure of the protein, which made the structure more stretchable. Similarly, Dai et al. [11] reported that while catechin concentration increased, the contents of α-helix and β-sheet in soy protein isolate decreased, whereas the contents of β-turn and random coil increased. In addition, a gradual blue-shift to a lower wavenumber in the range of amide II groups (1550–1510 cm^{-1}) was observed while EGCG ratio was increasing. These shifts might be attributed to the intermolecular forces between polyphenols and proteins, such as hydrophobic interaction [22].

Antioxidative properties of the protein–polyphenol conjugates

DPPH Radical scavenging activity

The ethanol solution of the stable free radical DPPH exhibited a deep violet hue. It showed significant 520 nm absorption. The violet color of DPPH hue dwindles or disappears after being neutralized by antioxidants. The antioxidant capacity of antioxidants was strongly correlated with the degree of color change. Consequently, DPPH was frequently employed to assess the antioxidant potency of antioxidants. The ability of the complexes with various polyphenol concentrations to scavenge DPPH radicals in comparison to pure polyphenols is shown in Fig. 5A. DPPH free radical scavenging activity of the complexes gradually increased while the EGCG, GA, or TA addition ratios were increasing, which were significantly higher than those of QG alone. Likewise, the DPPH free radical scavenging rate of the complexes was noticeably higher than that of pure EGCG and GA at the same concentration. This suggested that QG, EGCG, and GA might enhance QG antioxidant action while polyphenols prevent oxidation. EGCG and GA interact with QG through their hydrophobicity to lessen the likelihood, polyphenol molecules might undergo pro-oxidation [28]. Ashwar and Gani [29] discovered that radical scavenging capacity was considerably improved in a dose-dependent manner when casein and whey proteins were conjugated with Sea Buckthorn Polyphenols.

ABTS radical scavenging activity

ABTS free radical was one of the excellent tools for the determination of antioxidant activity in vitro. It was obtained by the reaction of ABTS diammonium salt with $K_2S_2O_8$ and had maximum UV absorption at 734 nm. Generally, the ABTS scavenging activity was comparable to the DPPH scavenging activity. As shown in Fig. 5B, after addition of EGCG, GA or TA, the ABTS free radical scavenging activity of the complex was significantly increased ($P < 0.05$), and increased with the increase of supplemental dose. The result indicated that EGCG, GA, and TA could enhance the antioxidant capacity of QG through non-covalent interaction, which could also be explained by the effect of the free hydroxyl group on the polyphenol after binding with protein.

Ferric reducing antioxidant power (FRAP)

The reducing power of a compound was also one of the criteria used to measure its antioxidant activity, which was usually judged by its ferric reducing antioxidant potential (FRAP). Figure 5C showed the FRAP values of QG and their complexes with various polyphenol concentrations and pure polyphenols. The addition of EGCG, GA, or TA to QG could greatly increase its reducing power. In the presence of EGCG, GA, or TA, the decreasing power of QG on DPPH and ABTS was nearly equal to or slightly lower than that of pure EGCG, GA, or TA at the same concentration. The antioxidant activity of the complexes was probably influenced by the bond dissociation enthalpy (BDE) of the O–H bond on the phenol and the crowding of the steric around the group in addition to the quantity of phenolic hydroxyl groups. While the electron with the attracting group increased the BDE, the electron with the providing group decreased it. The antioxidant stability of the complexes would be preserved or enhanced if polyphenols were covalently linked to electron-donating groups on proteins. Similar outcomes had been observed for complexes created by non-covalent interactions between polyphenols and moderate electron donors like aromatic amino acids [12]. Therefore, the effects of combining polyphenols with various amino acid residues can vary.

Conclusions

The formation of QG complex with EGCG, GA, or TA was confirmed by UV–Vis absorption spectra, particle size, and potential. The fluorescence findings demonstrated that the three polyphenols on QG used static quenching as their fluorescence quenching mechanism. Thermodynamic information demonstrates that the hydrophobic interactions between QG and EGCG, GA, or TA are endothermic and spontaneous. FTIR analysis further showed the change of secondary structure, the percentage of β-fold decreased, and the percentage of β-corner increased. In addition, antioxidant analysis showed that the combination of QG with EGCG, GA, or TA significantly improved DPPH and ABTS free radical scavenging abilities and Ferric reducing antioxidant power. Therefore, the antioxidant activity of quinoa glycopeptides can be enhanced through non-covalent interactions with polyphenols. The results provide a scientific basis for further study on the development of functional foods from quinoa peptides.

Acknowledgements This work was supported by the Zhejiang Province Top priority first-level discipline funding project (Grant No. 2017SIAR221).

Author contributions YY: conceptualization, data curation, formal analysis, funding acquisition, investigation, methodology, visualization, writing-original draft. SY: conceptualization, data curation, funding acquisition, methodology, project administration, resources, supervision, writing—review and editing.

Data availability Data will be made available on request.

Declarations

Competing interests The authors declare that they have no known competing financial interests or personal relationships that could have influenced the work reported in this paper.

References

1. N.A. Al-Shabib, J.M. Khan, A. Malik, M.T. Rehman, N. Altwaijry, Saudi Pharm. J. **28**(3), 238–245 (2020). https://doi.org/10.1016/j.jsps.2020.01.002
2. X.W. Wang, R.Y. Zhao, W.Q. Yuan, J. Cereal Sci. **95**, 103036 (2020). https://doi.org/10.1016/j.jcs.2020.103036
3. N.A. Mir, C.S. Riar, S. Singh, Food Struct. **28**, 100189 (2021). https://doi.org/10.1016/j.foostr.2021.100189
4. S.L. Li, C. Chen, Y.X. Ji, J. Lin, X.M. Chen, B. Qi, J. Cereal Sci. **84**, 83–89 (2018). https://doi.org/10.1016/j.jcs.2018.10.008
5. H.A. Suleria, C.J. Barrow, F.R. Dunshea, Foods **9**(9), 1206 (2020). https://doi.org/10.3390/foods9091206
6. G. Giuberti, G. Rocchetti, L. Lucini, Curr. Opin. Food Sci. **31**, 102–113 (2020). https://doi.org/10.1016/j.cofs.2020.04.003
7. J. Jiang, Z.P. Zhang, J. Zhao, Y.F. Liu, Food Chem. **268**, 334–341 (2018). https://doi.org/10.1016/j.foodchem.2018.06.015
8. Y. You, L. Yang, H. Chen, L. Xiong, F. Yang, J. Agric. Food Chem. **69**(7), 2306–2315 (2021). https://doi.org/10.1021/acs.jafc.0c07337
9. T.T. Dai, D.J. McClements, T. Hu, J. Chen, X.M. He, C.M. Liu, J.F. Sheng, J. Sun, Food Chem. **377**, 131950 (2022). https://doi.org/10.1016/j.foodchem.2021.131950
10. T.H. Quan, S. Benjakul, Colloids Surf. A **579**, 123711 (2019). https://doi.org/10.1016/j.colsurfa.2019.123711
11. S.C. Dai, Z.T. Lian, W.J. Qi, Y.S. Chen, X.H. Tong, T. Tian, B. Liu, M.M. Wang, H. Wang, L.Z. Jiang, Food Chem. **384**, 132507 (2022). https://doi.org/10.1016/j.foodchem.2022.132507
12. S. Parolia, J. Maley, R. Sammynaiken, R. Green, M. Nickerson, S. Ghosh, Food Chem. **367**, 130603 (2022). https://doi.org/10.1016/j.foodchem.2021.130603
13. C.Z. Liu, N. Lv, G.R. Ren, R.B. Wu, B.J. Wang, Z.X. Cao, H.J. Xie, Food Hydrocolloids **120**, 106906 (2021). https://doi.org/10.1016/j.foodhyd.2021.106906
14. X. Han, Z.Q. Liang, S.F. Tian, L. Liu, S. Wang, Food Res. Int. **158**, 111534 (2022). https://doi.org/10.1016/j.foodres.2022.111534
15. S.R. Wang, X.Y. Li, J.S. Zhu, H.C. Liu, T. Liu, G.P. Yu, M.L. Shao, J. Agric. Food Chem. **69**(27), 7777–7785 (2021). https://doi.org/10.1021/acs.jafc.1c01949
16. C. Pascal, C. Poncet-Legrand, B. Cabane, A. Vernhet, J. Agric. Food Chem. **56**(15), 6724–6732 (2008). https://doi.org/10.1021/jf800790d
17. F. Yi, K. Wu, G. Yu, C. Su, Colloids Surf. B **206**, 111954 (2021). https://doi.org/10.1016/j.colsurfb.2021.111954
18. Y.Y. Li, H.T. Liu, Q. Liu, B.H. Kong, X.P. Diao, Food Hydrocolloids **87**, 149–157 (2019). https://doi.org/10.1016/j.foodhyd.2018.07.052
19. F.C. Zhan, J.C. Yang, J. Li, Y.T. Wang, B. Li, Food Hydrocolloids **75**, 81–87 (2018). https://doi.org/10.1016/j.foodhyd.2017.09.010
20. J.H. Xu, M.H. Hao, Q.F. Sun, L. Tang, Int. J. Biol. Macromol. **136**, 804–812 (2019). https://doi.org/10.1016/j.ijbiomac.2019.06.053
21. X.H. Yan, Y.F. Gao, S.C. Liu, G.H. Zhang, J.X. Zhao, D. Cheng, Z.L. Zeng, X.F. Gong, P. Yu, D.M. Gong, Food Chem. **352**, 129377 (2021). https://doi.org/10.1016/j.foodchem.2021.129377
22. K. Liu, X.Q. Zha, Q.M. Ll, L.H. Pan, J.P. Luo, Food Hydrocolloids **118**, 106807 (2021). https://doi.org/10.1016/j.foodhyd.2021.106807
23. M. Zembyla, B.S. Murray, S.J. Radford, A. Sarkar, J. Colloid Interface Sci. **548**, 88–99 (2019). https://doi.org/10.1016/j.jcis.2019.04.010
24. Q.D. Xu, Z.L. Yu, W.C. Zeng, Food Res. Int. **148**, 110593 (2021). https://doi.org/10.1016/j.foodres.2021.110593
25. C.Z. Liu, N. Lv, Y.Q. Xu, H.F. Tong, Y.L. Sun, M. Huang, G.R. Ren, Q. Shen, R.B. Wu, B.J. Wang, Food Hydrocolloids **133**, 108022 (2022). https://doi.org/10.1016/j.foodhyd.2022.108022
26. Y.J. Zhang, N. Zhang, X.H. Zhao, Food Chem. **364**, 130375 (2021). https://doi.org/10.1016/j.foodchem.2021.130375
27. X. Li, T.T. Dai, P. Hu, C.H. Zhang, J. Chen, C.M. Liu, T. Li, Food Hydrocolloids **105**, 105761 (2020). https://doi.org/10.1016/j.foodhyd.2020.105761
28. T.T. Dai, J. Chen, D.J. McClements, P. Hu, X.Q. Ye, C.M. Liu, T. Li, Food Funct. **10**(2), 765–774 (2019). https://doi.org/10.1039/C8FO02246A
29. B.A. Ashwar, A. Gani, ACS-Food Sci. Technol. **1**(7), 1206–1214 (2021). https://doi.org/10.1021/acsfoodscitech.1c00103